Different protonated states at the C-terminal of the amyloid-β peptide modulate the stability of S-shaped protofibril

Xiuhua Yin, Shengtang Liu, Jose Manuel Perez-Aguilar (iD), Hong Zhou, Qiwen Shao, Zaixing Yang (iD), and Ruhong Zhou (iD)

View Online   Export Citation   CrossMark

ARTICLES YOU MAY BE INTERESTED IN

The Journal
of Chemical Physics

Submit Today

The Emerging Investigators Special Collection and Awards
Recognizing the excellent work of early career researchers!

AIP Publishing

Different protonated states at the C-terminal of the amyloid-β peptide modulate the stability of S-shaped protofibril

View Online   Export Citation   CrossMark

Xiuhua Yin,[1] Shengtang Liu,[1] Jose Manuel Perez-Aguilar,[2] (ID) Hong Zhou,[1] Qiwen Shao,[1] Zaixing Yang,[1,a)] (ID) and Ruhong Zhou[1,2,3,a)] (ID)

AFFILIATIONS

[1] Institute of Quantitative Biology and Medicine, State Key Laboratory of Radiation Medicine and Protection, School of Radiation Medicine and Protection, Collaborative Innovation Center of Radiological Medicine of Jiangsu Higher Education Institutions, Soochow University, Jiangsu 215123, China
[2] IBM Thomas J. Watson Research Center, Yorktown Heights, New York 10598, USA
[3] Department of Chemistry, Columbia University, New York, New York 10027, USA

a)Authors to whom correspondence should be addressed: ruhongz@us.ibm.com and zxyang@suda.edu.cn

ABSTRACT

Studies have found strong correlations between polymorphism and structural variations in amyloid-β (Aβ) fibrils and the diverse clinical subtypes of Alzheimer's disease (AD). Thus, a detailed understanding of the conformational behavior of Aβ fibrils may be an aid to elucidate the pathological mechanisms involved in AD. However, a key point that has been inadvertently underestimated or dismissed is the role of the protonated state at the C-terminal residue of amyloid-β peptides, which can give rise to intrinsic differences in the morphology and stability of the fibrils. For instance, the effects of the salt bridge formed between the C-terminal residue A42 and the residue K28 on the S-shaped Aβ protofibril structure remain unknown and may be different from those in the U-shaped Aβ protofibril structures. To address this effect, we explore the stability of the S-shaped protofibrils capped with different C-terminal modifications, including carboxyl group in its deprotonated (COO^-) and protonated (COOH) states, by using molecular dynamics simulations. Our findings indicated that the C-terminal deprotonated protofibril is significantly more stable than its C-terminal protonated counterpart due to a well-defined and highly stable zipper-like salt-bridge-chain formed by the ε-NH_3^+ groups on the sidechain of residue K28 and the C-terminal COO^- group at the A42 residue. The revealed underlying molecular mechanism for the different stability of the protofibrils provides insights into the diversity of polymorphism in Aβ fibrils.

Published under license by AIP Publishing. https://doi.org/10.1063/1.5081948

INTRODUCTION

Polymorphism is a phenomenon commonly encountered in a variety of amyloid fibrils and is related to various neurodegenerative diseases, such as Alzheimer's disease (AD),[1] diabetes type II,[2,3] and Huntington disease (HD).[4,5] Recent studies have shown that AD exhibits a wide spectrum of Amyloid-β (Aβ) structural states. In general, Aβ is a 39- to 42-residue peptide produced through the cleavage of the amyloid precursor protein (APP) by the β and γ-secretases[6,7] and subsequently released into extracellular[8] or intracellular milieu.[9] Aggregation of amyloid-β peptides into amyloid fibrils or plaques is part of the hallmarks of Alzheimer's disease (AD).[10] The most prominent forms of Aβ peptides are the Aβ$_{1-40}$ and Aβ$_{1-42}$ species, which only differ by two amino acids (Ile41 and Ala42) at the C-terminus. These two Aβs can further form insoluble fibrils found in extracellular amyloid plaques in the AD brain, and it is known that the Aβ$_{1-42}$ peptide aggregates faster and is more neurotoxic than the Aβ$_{1-40}$ counterpart.[11-13]

Moreover, the different conformers of Aβ may also play a pivotal role in the pathogenesis of distinct AD phenotypes.[14,15] Hence, a detailed comprehension of the Aβ structure and its conformational behaviors is critical to understand the aggregation process

and subsequent disease development. However, due to its inherent properties, i.e., intrinsic disorder and low solubility, the Aβ peptides cannot be subjected to crystallization. Thus, the structural information on the oligomeric states of Aβ remains sparse. The current three major types of Aβ 3D structures, namely, U-shaped, S-shaped, and tilde-shaped (supplementary material, Table S1), were determined by advanced technologies, such as solid-state nuclear magnetic resonance and cryoelectron microscopy.[16–20] Two specific regions in the Aβ peptide sequence seem to play crucial roles in the formation of specific Aβ protofilaments: one is the central basic or acidic residues (i.e., K28 and E22/D23, respectively), which is capable of forming salt bridges; the other is the specific modification of its C-terminus, which play a significant role in the central salt bridge formation in the fibril structures.[21] In this context, Luhrs et al.[16] obtained the U-shaped structural motif using Aβ$_{1-42}$ peptides where the C-terminus was amidated (CONH$_2$) and observed the formation of a salt bridge between the K28 and D23 residues. By contrast, several studies using the same Aβ$_{1-42}$ peptide, but where the C-terminus was left with the standard moiety (deprotonated carboxylic group, COO$^-$), produced the S-shaped structure and a different salt bridge interaction (in this case, between K28 and the A42 terminal carboxylate).[18,19,22] Finally, under conditions where the terminal carboxylate is protonated (COOH), the Aβ$_{1-42}$ peptide formed the tilde-shaped structure but as expected, the salt bridge interaction between the K28 and the A42 terminal moiety is absent.[17,23]

A comprehensive literature review revealed that the characterization of the S-shaped structure, and particularly its C-terminal salt bridge interaction, may help us in understanding the other two

structural types of the Aβ$_{1-42}$ peptide. Due to the computational resources needed to study the aggregation process of the Aβ$_{1-42}$ peptide using atomistic simulations, we focus our current attention in the characterization of the stability and conformational features of the S-shaped Aβ structure and the role of the presence of different chemical groups at the C-terminus.

MODELS AND METHODS

We built an S-shaped initial Aβ fibril model based on a segment of the dimeric fibril structure reported by Michael et al. (PDB ID: 5KK3)[19] that contained nine Aβ$_{11-42}$ peptides. As shown in Fig. 1(a), the native S-shaped Aβ$_{11-42}$ protofibril contains a smaller hydrophobic core (named "hydrophobic-core-A," including G29, I31, G33, V36, V39, and I41) and a larger hydrophobic core (named "hydrophobic-core-B," including L17, F19, F20, V24, N27, A30, and A32). Each peptide also forms a three stranded β-sheet with strands β1 of residues 12–18, β2 of residues 24–33, and β3 of residues 36–40. In the current study, we investigated the S-shaped Aβ peptide structure capped with two different chemical groups at the C-terminus: carboxyl group in the deprotonated (COO$^-$) and protonated (COOH) states. On the other hand, the pKa values of the two different C-terminal protonated peptides were computed using the PROPKA 3.1 program.[24] The results demonstrate that there was no distinctive pKa shift for all titratable residues between two different C-terminal protonated state peptides (Table S2).

First, the nine Aβ$_{11-42}$ peptides were solvated in a 6.72 nm × 7.42 nm × 8.73 nm water box with approximately 12 460 water

(a)

| 11 | | | | 21 | | | | 31 | | | | 42 |

E V H H Q K L V F F A E D V G S N K G A I I G L M V G G V V I A

(b)

A42-COO$^-$ A42-COOH
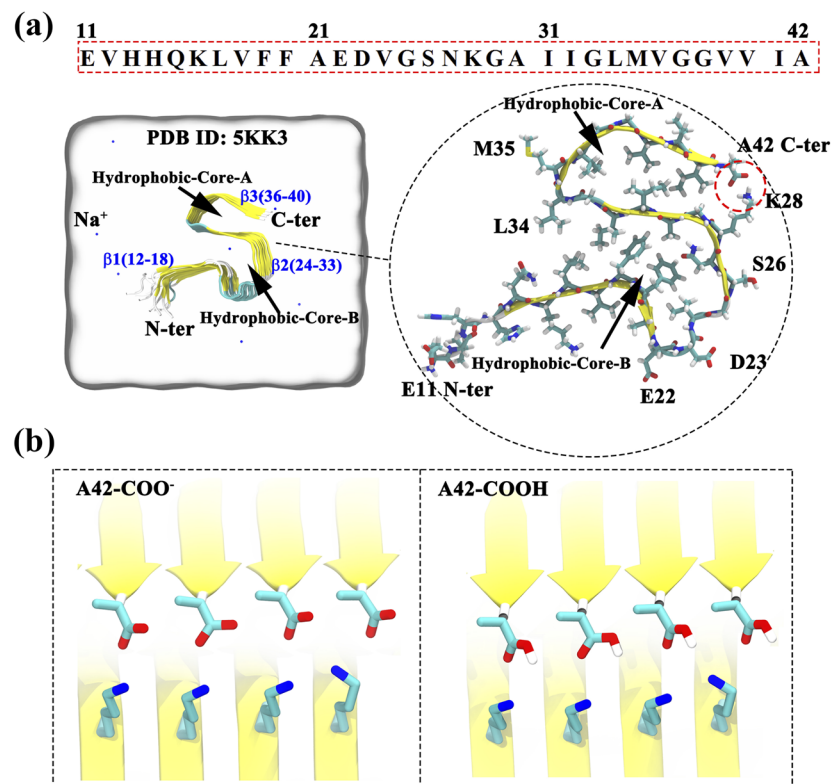
FIG. 1. The initial configuration of the simulated system consisting of the S shape Aβ$_{11-42}$ peptide embedded in the water solvated system. (a) The sequence and the structural features S shape Aβ$_{11-42}$ protofibril. The Aβ$_{11-42}$ protofibril inserted in the cubic water box (6.72 nm × 7.42 nm × 8.73 nm) and represented as the "NewCartoon" model, Na$^+$ as the counter ions to neutralize the simulation system are shown as blue sphere. (b) The C-terminal of each Aβ$_{11-42}$ peptide is capped with the standard C-terminus (COO$^-$) and protonated C-terminus (COOH). For clarity, some hydrogen atoms are not shown.

molecules; then, nine sodium ions were added to neutralize the system (as detailed in Fig. 1). All simulation systems were built and visualized using the VMD[25] program (version 1.9.2). The simulations were performed using the GROMACS (version 4.6.7) package[26] with the CHARMM27 force field.[27,28] The TIP3P water model[29] was applied for water molecules. The system was then minimized by 5000 steps, followed by a 1 ns equilibration, in which all heavy atoms of peptides are restrained. During the equilibration and production runs, the temperature and pressure were maintained at 300 K and at 1 atm by using a modified Berendsen thermostat[30] and Parrinello–Rahman barostat,[31] respectively. The long-range Coulomb interactions were treated by the particle mesh Ewald (PME) method,[32] whereas van de Waals interactions were handled with a smooth cutoff distance of 1.2 nm. Five independent 100 ns long production runs were carried out for each of the four different C-terminal modifications that resulted in a total aggregate simulation time of 2 μs under the NPT ensemble. The equation of motion was integrated with a time step of 2.0 fs, and coordinates were collected every 2.0 ps. The secondary structure analysis of the protofibril structures was calculated using the dictionary of the protein secondary structure[33] protocol available in the do_dssp module of the GROMACS package.

The potential of mean force (PMF) profile of a single peptide to its parent protofibril was estimated using the umbrella sampling method.[34,35] The reaction coordinate was defined as the distance (from 0.4 nm to 5.0 nm) of the peptide center of mass to its parent protofibril along with the long-axis of protofibril. The harmonic potential with a force constant of 2000 kJ mol^{-1} nm^{-2} was applied on the peptide. The reaction path was divided into 47 windows, with each simulating for 5 ns. The Weighted Histogram Analysis Method (WHAM)[36,37] was applied to calculate the PMF. All PMF profiles were offset by its value at the distance of 5.0 nm, where the PMF reached a constant. The statistical uncertainty of the PMF was estimated by bootstrapping analysis[38] with an equilibration phase of 1 ns in length.

RESULTS AND DISCUSSIONS

The present study focuses on the role of the different protonated states of residue A42 at the C-terminus of the peptide on the stability of the S-shaped Aβ_{11-42} protofibril. Therefore, our attentions are mainly devoted to the direct correlation between the stability of "hydrophobic-core-A" and the "K28-NH$_3^+$-A42-COO$^-$" salt bridge since the hydrophobic-core-A is wrapped at the end of the peptide by the K28-NH$_3^+$-A42-COO$^-$ interaction. In this study, we present the simulation results for the effects of two types of C-terminal modifications in the stability of the Aβ_{11-42} protofibrils. First, we constructed a conformational free energy surface with regard to the stability of two protofibrils. Then, we compared the dynamical properties of the two protofibrils. Finally, the possible mechanisms that cause distinct structural stability level were proposed.

The structural stability of the two Aβ_{11-42} protofibrils with different C-terminal protonated states was examined by the protofibril conformational free energy surface (FES) (potential of mean force). Here, the two dimensional FES was constructed along the root mean square distance (RMSD) and the solvent accessible surface area (SASA) by $\Delta G(RMSD, SASA) = -K_b T \ln P(RMSD, SASA)$, where K_b

is the Boltzmann constant, T is the temperature, $P(RMSD, SASA)$ is the probability of the configuration of protofibril locating at the coordinate of ($RMSD$, $SASA$). Here, SASA measures the degree of exposure of the Aβ_{11-42} protofibril to solvent (water), so a larger SASA value indicates a more swelled protofibril structure. RMSD reflects the structural similarity of the Aβ_{11-42} protofibril to its crystal structure. Thus, a larger RMSD value demonstrates a larger protofibril structural deviation. The overlap in FES distribution spaces and the convergence of FES are also analyzed. The exact steps are as follows: first, all configurations from all independent trajectories are randomly divided into 10 data subsets; second, three out of ten data subsets are extracted and be used to construct three sub-FESs for assessing the overlap and convergence of FESs; finally, the final FES is constructed by averaging over the all 10 data subsets. The statistical sampling error in FES is estimated using the bootstrapping scheme[38] by calculating the standard deviation (SD) between the ten data sets.[37,39] Meanwhile, the representative configuration corresponds to the energy minimum is captured and rendered in terms of the protein surface and "Newcartoon" model using the VMD program[25] to show the overall structure and the secondary structure of the protofibril.

We first validate the overlap and convergence of the FES distribution. The two sets of three sub-FESs clearly demonstrate that the conformational FES distribution for both the C-terminal deprotonated and protonated Aβ_{11-42} protofibrils is overlapped very well (Fig. S1). Particularly, the exact FES distribution patterns (including the specific coordinate space of the distribution and the exact local/global energy minimum value) in the three sub-FESs for the C-terminal deprotonated and protonated Aβ_{11-42} protofibrils are very closer, indicating a reasonable convergence of the FES distributions.

Next, we study the thermodynamic stability of the two different C-terminal protonated states Aβ_{11-42} protofibril. As shown in Figs. 2(a) and 2(b), the distributions of the FES for the two different Aβ_{11-42} protofibrils hydrophobic-core-A are largely different. In the case of C-terminal deprotonated protofibril [Fig. 2(a); A42-COO$^-$, the native state], there is only one free energy basin; the FES displays a compact "native-like" state around the basin, indicating the convergence of the fibrillar hydrophobic-core-A structure. At the basin (0.40 nm, 47 nm^2), with $\Delta G = -15.0 \pm 0.1$ kJ/mol, the overall structure of the protofibril is intact, with only one edge β3-sheet partially broken. Then, we superimposed the configurations of the simulated trajectories at 1 ns interval and found that the integral structural deviation is very small [Fig. 2(c)]. Moreover, by measuring the secondary structure variation of the integral protofibril, it also demonstrated a very tiny reduction in β-sheet content [only decreased by ~0.07, Fig. 2(d)].

As for the case of the C-terminal protonated protofibril (A42-COOH), the distribution of the FES is much broader and more complicated. As displayed in Fig. 2(b), there are two free energy basins distributed over the FES. The first minimum is located at (0.45 nm, 51 nm^2), with $\Delta G = -13.4 \pm 0.1$ kJ/mol. In this state, the surface of the protofibril is very rough, with the hydrophobic-core-A partially impaired. Also, more edge β3-sheets (highlighted by the red circle) detach from the protofibril, accompanied by the formation of a loosely packed inner core of the protofibril (with a small "crack"). The second minimum is located at (0.67 nm, 52 nm^2), with $\Delta G = -12.6 \pm 0.2$ kJ/mol. In this state, the crack became much larger, the
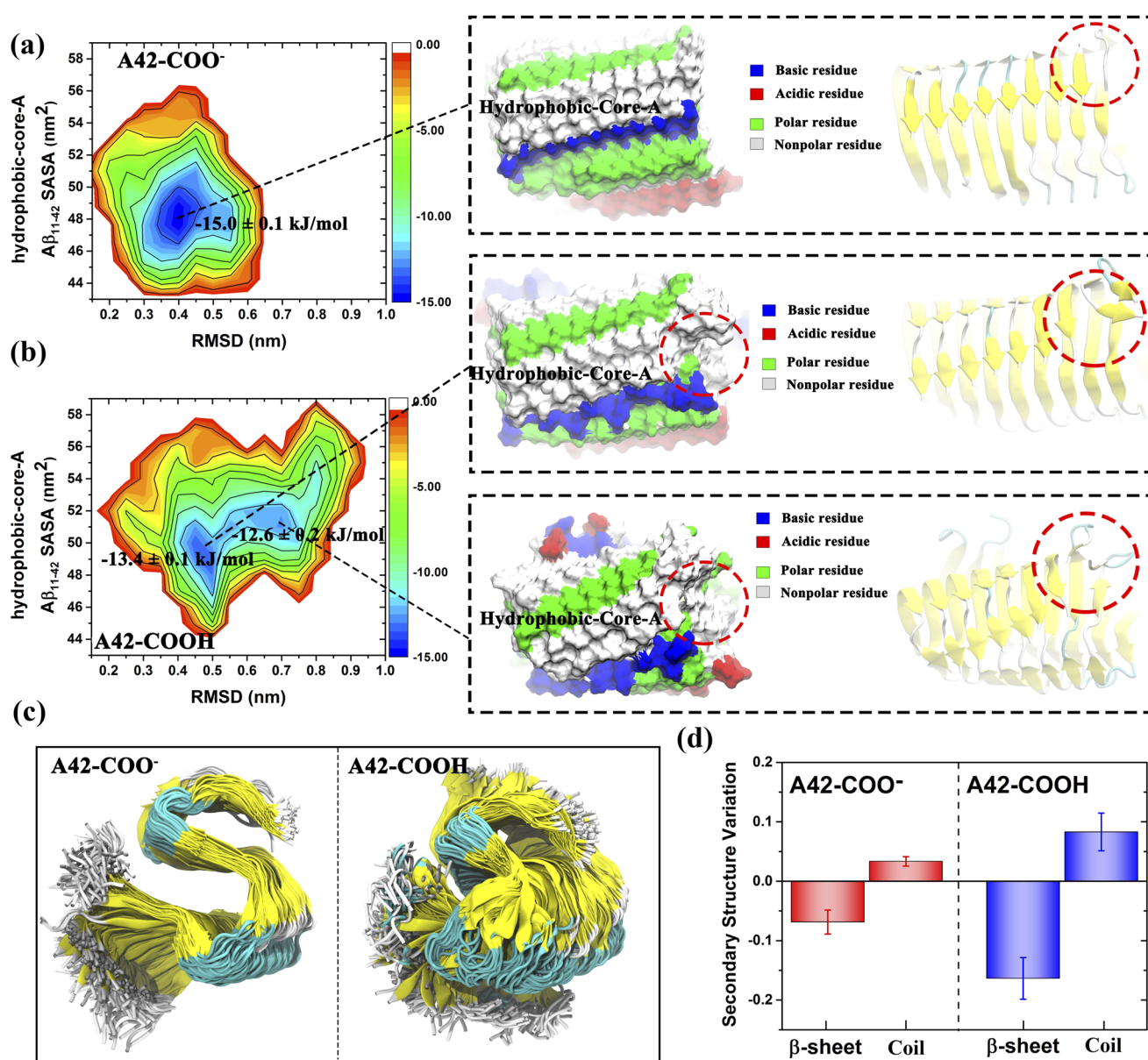
FIG. 2. [(a) and (b)] The conformational free energy surface of the C-terminal deprotonated and protonated Aβ$_{11–42}$ protofibrils, and typical protofibril configuration(s) that correspond(s) to the free energy basin(s). (c) The protofibril structure superimposed by the extracted configurations from the trajectories of the two systems at 1 ns interval. Left for the C-terminal deprotonated protofibril, while right the for C-terminal protonated protofibril. (d) The comparison of the β-sheet content between the initial protofibril structure and that at the equilibrium state (last 50 ns).

hydrophobic-core-A was further disrupted, and the β3-sheet formed by the detached two strands completely disappeared. Moreover, the superimposed integral protofibril structure that extracted from the trajectories at 1 ns interval also displayed a very large deviation [Fig. 2(c)]. The β-sheet content of the integral protofibril sharply decreased by ~0.17, which is about more than twice of which in the case of the C-terminal deprotonated protofibril [Fig. 2(d)].

Therefore, we can conclude that the C-terminal protonated state can significantly affect the thermodynamic stability of the Aβ$_{11–42}$ protofibril. More specifically, the C-terminal deprotonated protofibril is much more stable than its C-terminal protonated counterpart.

We further examined the time evolution of the conformation of the two Aβ$_{11–42}$ protofibrils with different C-terminal protonated

states, which might offer an overall view on their structural stability differences and provide a microscopic picture of the underlying mechanisms. Here, the RMSD [Fig. 3(a)], hydrophobic-core-A SASA [Fig. 3(b)], together with the key configurations [Fig. 3(c)] at the critical time points were applied to measure the structural stability of the protofibril.

In general, the conformational adjustment process of the C-terminal protonated protofibril is more complicated than its C-terminal deprotonated counterpart. In the case of the C-terminal deprotonated protofibril, the most significant protofibril conformational change only occurs in a single stage, despite the exact time scale varying in different trajectories (Figs. 3 and S2). Herein, we take a trajectory as an example to show the conformational shifting process [Figs. 3(a) and 3(c)]. During the adjustment stage (<20 ns), the original relatively flat fibrillar morphology became a left-hand twist pattern, which make the protofibril RMSD

value increased by ~0.2 nm, and the hydrophobic-core-A SASA value decreased slightly by ~4 nm^2. This is reasonable. The initial relative loose configuration of the C-terminal deprotonated protofibril was obtained from the crystal structure resolved by the ssNMR at the gas phase. When it is solvated in water, the hydrophobic effect and the other protein intrinsic forces (such as van der Waals and electrostatic) inevitably drive the protofibril to make some spatial adjustments to become more compact to accommodate the aqueous environment. It is noteworthy that at the end of the simulation, the edge β3-sheet around the hydrophobic-core-A was partially disrupted, but the hydrophobic-core-A maintained intact [see the top panel figures in Fig. 3(c)].

On the other hand, the C-terminal protonated protofibril displayed a two-stage protofibril conformational change pattern in three out of five runs (run 3–5) (Figs. 3 and S3). Similarly, we also take a trajectory to describe those conformational behaviors
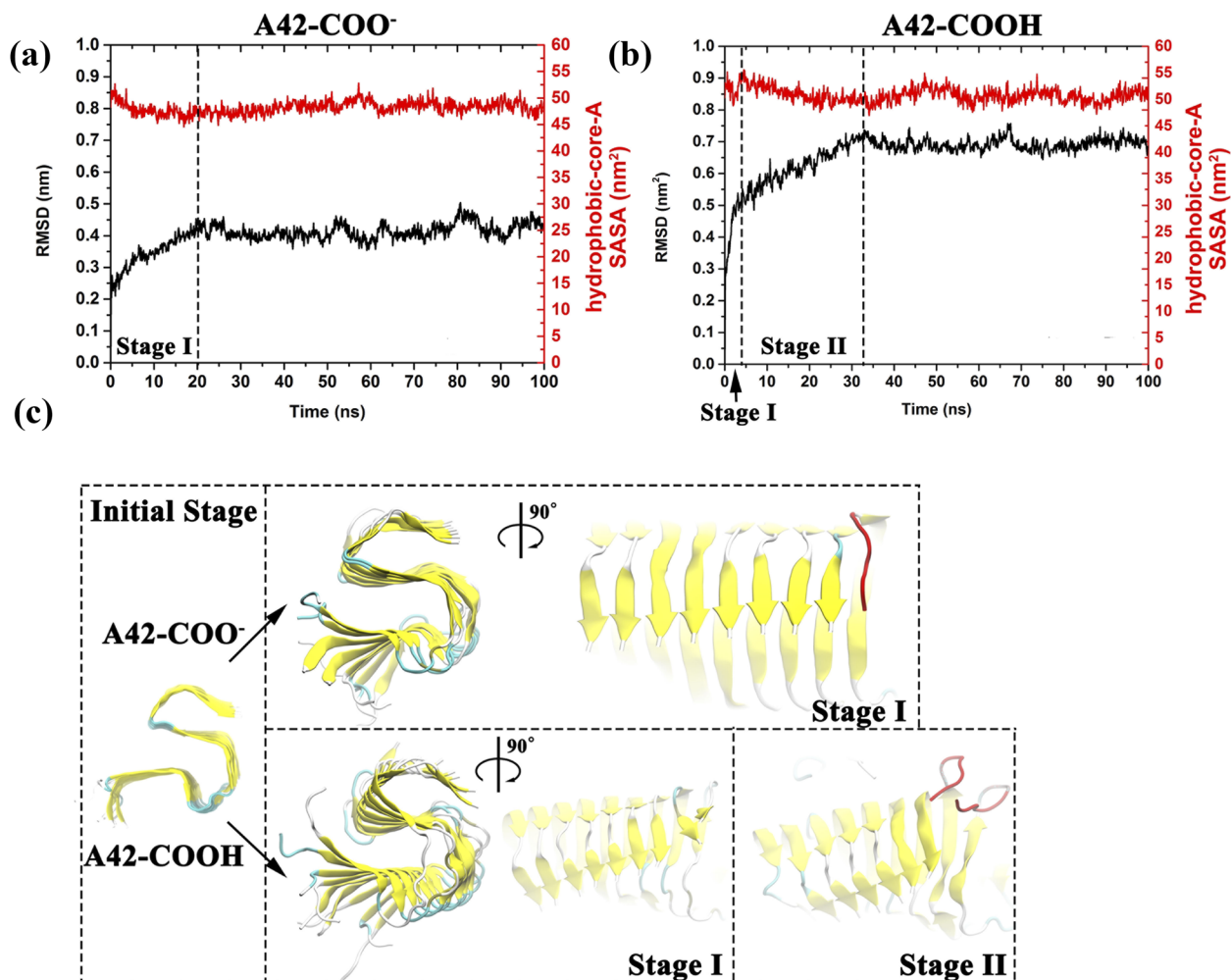

FIG. 3. [(a) and (b)] Time evolution of the RMSD and the hydrophobic-core-A SASA values to measure the structural dynamical properties of the two different C-terminal protonated Aβ$_{11-42}$ protofibrils. (c) Some snapshots at key simulation time points to illustrate the crucial structural changes during the simulations (see Figs. S4 and S5 for more details).

[Figs. 3(b) and 3(c)]. At the stage I (<4 ns), the RMSD value already increased sharply by ~0.50 nm and the hydrophobic-core-A SASA value decreased by ~2 nm^2, when the fibrillar morphology became a left-hand twist pattern. Meanwhile, the β3 segments on the two edge strands partially separate from the protofibril and become more flexible in water, which induce the hydrophobic-core-A SASA value increased by ~6 nm^2 and introduce an apparent "crack" to the hydrophobic-core-A. This is to say, water molecules can directly attack the hydrophobic-core-A from now on. During the stage II (from ~4 to ~34 ns), a larger hydrophobic-core-A area is exposed to water and became disrupted, which in turn induced the two β3 segments to fully detach from the protofibril with their β-sheet structure completely vanished. These conformational changes collectively resulted in the increase in the RMSD value from ~0.53 to ~0.72 nm. The overall structure of the protofibril simultaneously became more twisted, which gives rise to the decrease in the hydrophobic-core-A SASA. Thereafter, this state remained until the end of the simulation. It is noteworthy that we did not directly observe the full destruction

of the protofibril under our current simulation time scale, but we speculate that the destruction should be more remarkable in the long run.

Analyses of the dynamical properties of the two Aβ$_{11-42}$ protofibrils with different C-terminal protonated states suggest that the breakage of the β3 segment from the protofibril and the exposure of hydrophobic-core-A to water are the key steps for the destruction of the protofibril (more below).

To further reveal the underlying molecular mechanism for the influence of the C-terminus protonated state on the stability of the β3 segment and hydrophobic-core-A of the Aβ$_{11-42}$ protofibril, we systematically investigated the structural characteristics of the C-terminal of the two Aβ$_{11-42}$ protofibrils and their hydrophobic-core-A at the final configurations (Fig. 4).

In the case of the C-terminal deprotonated protofibril [Fig. 4(a)], the alternatively arranged A42-COO$^-$ groups and the ε-NH$_3^+$ groups on the sidechain of K28 construct a well-defined and highly stable zipper-like salt-bridge-chain, which is maintained
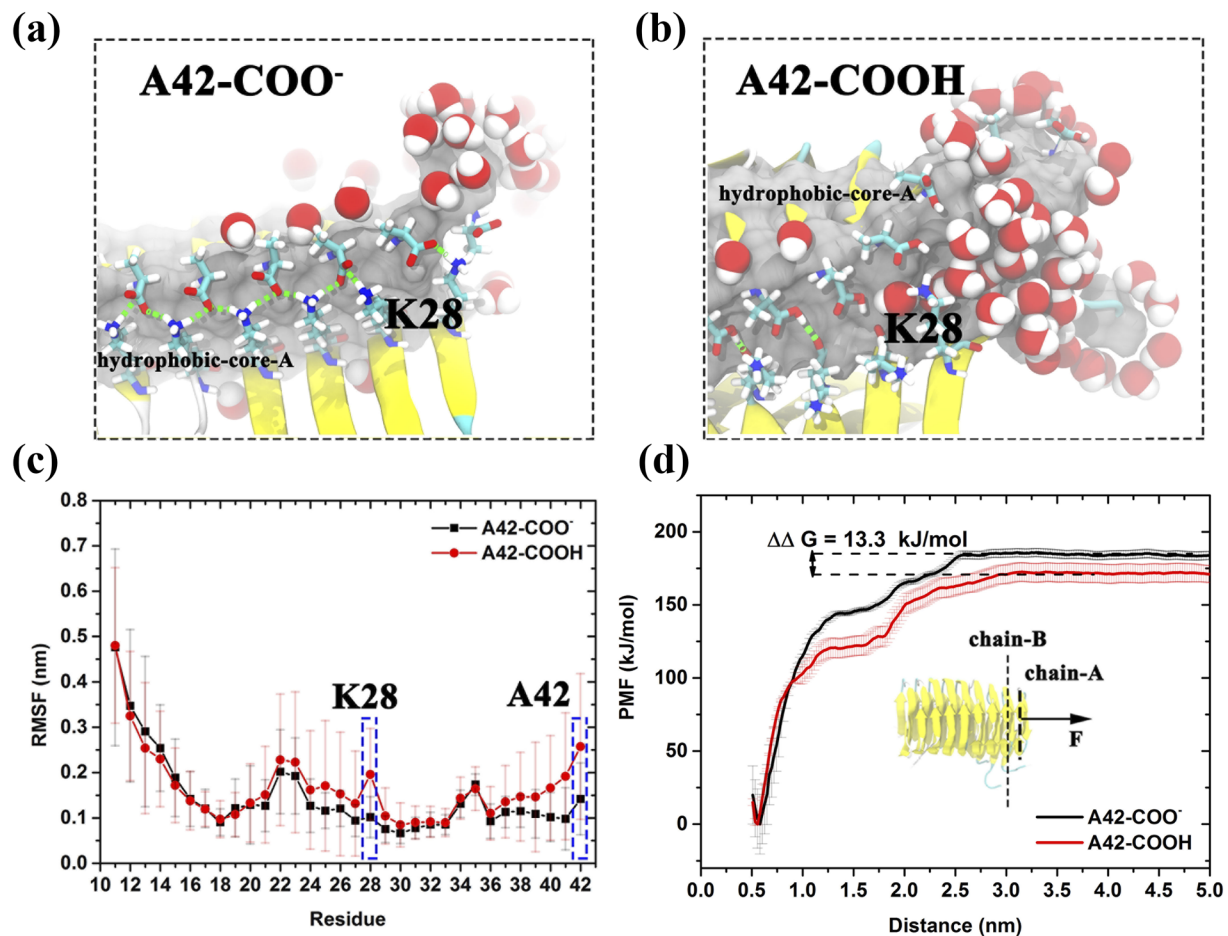

FIG. 4. Interior and exterior interactions of Aβ$_{11-42}$ peptides and various structural properties of the protofibrils with different C-terminal capping groups. (a) For the C-terminal deprotonated protofibril and (b) for the C-terminal protonated protofibril. (c) The difference in residual root mean square fluctuation (RMSF) between two different Aβ$_{11-42}$ protofibrils, where the values for residues K28 and A42, are highlighted by blue frames. (d) The PMF profiles to show binding free energies of a C-terminal protonated/deprotonated peptide to the C-terminal protonated/deprotonated protofibril.

very well until the very end of the simulation. On the one hand, this unique salt-bridge-chain remarkably reinforces the associations between the two adjacent peptides and intactly harbors the hydrophobic-core-A from being directly attacked by water. On the other hand, it also tightly anchors the C-terminals (A42-COO$^-$) of the peptide onto the main body of the protofibril. These factors worked together to effectively suppress the fluctuations of the C-terminal of the peptide [Fig. 4(c), black curve] and significantly stabilize the overall structure of the protofibril. Whereas, in the case of the C-terminal protonated protofibril, the specificity and strength of the interactions between the polar A42-COOH groups and ε-NH$_3^+$ groups on the sidechain of K28 are much weaker as compared to its deprotonated counterpart. This induces the arrangement of A42-COOH groups, and the sidechain of K28 becomes more disordered [Fig. 4(b)] and flexible [Fig. 4(c), red curve]. Hence, under the continuous attack of the water molecules, the β3 segments on the two edge strands gradually detach from the protofibril. Then, more and more water molecules intrude into the hydrophobic-core-A of the protofibril, resulting in the separation of the two β3 segments. As thus, the stability of the C-terminal protonated protofibril is largely reduced.

To validate the above assumptions, the binding free energies (potential mean force, PMF) of a single peptide to a parent protofibril with the C-terminal protonated or deprotonated are comparatively studied by using umbrella-sampling method. As shown in Fig. 4(d), the binding free energy for the C-terminal deprotonated peptide to its parent protofibril (~185.7 ± 2.8 kJ/mol) is much stronger than its protonated counterpart (~172.4 ± 6.2 kJ/mol). Obviously, the enhanced peptide binding affinity (~13.3 kJ/mol) and stability of the C-terminal deprotonated protofibril are the consequences of the deprotonated state at the end of peptide C-terminus. This result strongly demonstrates that the unique K28-NH$_3^+$-A42-COO$^-$ salt bridge in the deprotonated peptide is an important contribution to the S-shaped Aβ fibrils structure maintenance and stability, which is in good agreement with experiments.[18,20,22]

It is interesting to note that Xi et al.[40] recently suggested that protofibril stability mainly depends on the hydrophobic contacts involving the C-terminal residues, rather than the special salt bridge K28-NH$_3^+$-A42-COO$^-$. The main proof was that the N-terminal β-motif (β2 and β3) is not fully dissolved in their simulation time scale (over 200 ns). However, they also observed that the hydrophobic-core-A was somewhat disrupted and obtained a similar RMSF profile of the K28A mutant protofibril to our protonated RMSF profile. As discussed above, we believe the lack of large destruction of the N-terminal β-motif is largely due to the shortage of the simulation time. Moreover, we propose that the role of the salt bridge and hydrophobic core on the stability of the protofibril is complementary. A highly stable ambient salt bridge chain can smoothly bridge the dry interior (hydrophobic-core-A) of the protofibril to the external aqueous environment and resist the invasion of water; on the other hand, an intact hydrophobic core can provide a stable scaffold for the salt bridge chain in return.

CONCLUSION

In this paper, we investigated the conformational consequences of the S-shaped structure with different C-terminal protonated states

by using atomistic molecular dynamics simulations. The native S-shaped Aβ$_{11-42}$ structure (deprotonated state) was significantly stabilized by a well-defined and highly stable zipper-like salt-bridge-chain formed by the ε-NH$_3^+$ groups on the sidechain of residue K28 and the C-terminal COO$^-$ group at the A42 residue. By contrast, when the C-terminal group at the A42 is protonated (–COOH), the protofibril became less stable. This difference is due to the lack of interpeptide electrostatic associations between the ε-NH$_3^+$ groups on the sidechain of residue K28 and the C-terminal COOH group. The protonated state at the C-terminus of peptide decreases interpeptide binding free energy. Despite the absence of a detailed pathway of the Aβ aggregation, the present study demonstrates that the protonated state in the peptide C-terminus plays an important role in determining the stability of the S-shaped structure of the Aβ protofibril. In the context of the polymorphic properties of the fibril and the complex process involving the Aβ aggregation pathway, our results suggest that the structural and physicochemical specifics in the physiological conditions, such as pH (thus the protonation states), may play a significant role.

SUPPLEMENTARY MATERIAL

See supplementary material for analysis of classification of Aβ$_{42}$ and Aβ$_{40}$ protofibrils, including prepare condition, salt bridge location and document information, pKa values for all titratable residues in the C-terminal protonated and deprotonated S-shaped A42 peptides, additional convergence tests for free energy surface distribution, time evolution of the RMSD and the hydrophobic-core-A SASA of the C-terminal deprotonated and protonated Aβ$_{11-42}$ protofibril, time evolution of the hydrophobic-core-A surface of Aβ$_{11-42}$ capped with COO$^-$ at C-terminus, and time evolution of the secondary structure of Aβ$_{11-42}$ protofibril capped with COO$^-$ and COOH.

ACKNOWLEDGMENTS

REFERENCES

[1]Y. Miller, B. Ma, and R. Nussinov, "Polymorphism in Alzheimer A beta amyloid organization reflects conformational selection in a rugged energy landscape," Chem. Rev. 110, 4820–4838 (2010).

[2]J. Madine, E. Jack, P. G. Stockley, S. E. Radford, L. C. Serpell, and D. A. Middleton, "Structural insights into the polymorphism of amyloid-like fibrils formed by region 20-29 of amylin revealed by solid-state NMR and x-ray fiber diffraction," J. Am. Chem. Soc. 130, 14990–15001 (2008).

[3]J. T. Nielsen, M. Bjerring, M. D. Jeppesen, R. O. Pedersen, J. M. Pedersen, K. L. Hein, T. Vosegaard, T. Skrydstrup, D. E. Otzen, and N. C. Nielsen, "Unique identification of supramolecular structures in amyloid fibrils by solid-state NMR spectroscopy," Angew. Chem., Int. Ed. 48, 2118–2121 (2009).

[4]H. Kang, F. X. Vazquez, L. L. Zhang, P. Das, L. Toledo-Sherman, B. Q. Luan, M. Levitt, and R. H. Zhou, "Emerging beta-sheet rich conformations in super-compact huntingtin exon-1 mutant structures," J. Am. Chem. Soc. **139**, 8820–8827 (2017).

[5]Y. Fu, P. Wu, Y. Pan, X. Sun, H. Yang, M. Difiglia, and B. Lu, "A toxic mutant huntingtin species is resistant to selective autophagy," Nat. Chem. Biol. **13**, 1152 (2017).

[6]B. De Strooper, P. Saftig, K. Craessaerts, H. Vanderstichele, G. Guhde, W. Annaert, K. Von Figura, and F. Van Leuven, "Deficiency of presenilin-1 inhibits the normal cleavage of amyloid precursor protein," Nature **391**, 387–390 (1998).

[7]W. P. Esler and M. S. Wolfe, "A portrait of Alzheimer secretases—New features and familiar faces," Science **293**, 1449–1454 (2001).

[8]L. Rajendran, M. Honsho, T. R. Zahn, P. Keller, K. D. Geiger, P. Verkade, and K. Simons, "Alzheimer's disease β-amyloid peptides are released in association with exosomes," Proc. Natl. Acad. Sci. U. S. A. **103**, 11172 (2006).

[9]T. Hartmann, S. C. Bieger, B. Brühl, P. J. Tienari, N. Ida, D. Allsop, G. W. Roberts, C. L. Masters, C. G. Dotti, K. Unsicker, and K. Beyreuther, "Distinct sites of intracellular production for Alzheimer's disease Aβ40/42 amyloid peptides," Nat. Med. **3**, 1016 (1997).

[10]C. L. Masters, G. Simms, N. A. Weinman, G. Multhaup, B. L. Mcdonald, and K. Beyreuther, "Amyloid plaque core protein in Alzheimer-disease and down syndrome," Proc. Natl. Acad. Sci. U. S. A. **82**, 4245–4249 (1985).

[11]G. Meisl, X. Yang, E. Hellstrand, B. Frohm, J. B. Kirkegaard, S. I. Cohen, C. M. Dobson, S. Linse, and T. P. Knowles, "Differences in nucleation behavior underlie the contrasting aggregation kinetics of the Abeta40 and Abeta42 peptides," Proc. Natl. Acad. Sci. U. S. A. **111**, 9384–9389 (2014).

[12]N. L. Fawzi, J. Ying, R. Ghirlando, D. A. Torchia, and G. M. Clore, "Atomic-resolution dynamics on the surface of amyloid-[bgr] protofibrils probed by solution NMR," Nature **480**, 268–272 (2011).

[13]C. Haass and D. J. Selkoe, "Soluble protein oligomers in neurodegeneration: Lessons from the Alzheimer's amyloid beta-peptide," Nat. Rev. Mol. Cell Biol. **8**, 101–112 (2007).

[14]M. L. Cohen, C. Kim, T. Haldiman, M. ElHag, P. Mehndiratta, T. Pichet, F. Lissemore, M. Shea, Y. Cohen, W. Chen, J. Blevins, B. S. Appleby, K. Surewicz, W. K. Surewicz, M. Sajatovic, C. Tatsuoka, S. L. Zhang, P. Mayo, M. Butkiewicz, J. L. Haines, A. J. Lerner, and J. G. Safar, "Rapidly progressive Alzheimer's disease features distinct structures of amyloid-beta," Brain **138**, 1009–1022 (2015).

[15]W. Qiang, W. M. Yau, J. X. Lu, J. Collinge, and R. Tycko, "Structural variation in amyloid-beta fibrils from Alzheimer's disease clinical subtypes," Nature **541**, 217–221 (2017).

[16]T. Luhrs, C. Ritter, M. Adrian, D. Riek-Loher, B. Bohrmann, H. Dobeli, D. Schubert, and R. Riek, "3D structure of Alzheimer's amyloid-beta(1-42) fibrils," Proc. Natl. Acad. Sci. U. S. A. **102**, 17342–17347 (2005).

[17]M. Schmidt, A. Rohou, K. Lasker, J. K. Yadav, C. Schiene-Fischer, M. Fandrich, and N. Grigorieff, "Peptide dimer structure in an Abeta(1-42) fibril visualized with cryo-EM," Proc. Natl. Acad. Sci. U. S. A. **112**, 11858–11863 (2015).

[18]Y. L. Xiao, B. Y. Ma, D. McElheny, S. Parthasarathy, F. Long, M. Hoshi, R. Nussinov, and Y. Ishii, "Abeta(1-42) fibril structure illuminates self-recognition and replication of amyloid in Alzheimer's disease," Nat. Struct. Mol. Biol. **22**, 499–U497 (2015).

[19]M. T. Colvin, R. Silvers, Q. Z. Ni, T. V. Can, I. Sergeyev, M. Rosay, K. J. Donovan, B. Michael, J. Wall, S. Linse, and R. G. Griffin, "Atomic resolution structure of monomorphic Aβ42 amyloid fibrils," J. Am. Chem. Soc. **138**, 9663–9674 (2016).

[20]L. Gremer, D. Scholzel, C. Schenk, E. Reinartz, J. Labahn, R. B. G. Ravelli, M. Tusche, C. Lopez-Iglesias, W. Hoyer, H. Heise, D. Willbold, and G. F. Schroder, "Fibril structure of amyloid-ss(1-42) by cryoelectron microscopy," Science **358**, 116 (2017).

[21]B. Chandra, V. S. Mithu, D. Bhowmik, A. K. Das, B. Sahoo, S. Maiti, and P. K. Madhu, "Curcumin dictates divergent fates for the central salt bridges in amyloid-beta40 and amyloid-beta42," Biophys. J. **112**, 1597–1608 (2017).

[22]M. A. Wälti, F. Ravotti, H. Arai, C. G. Glabe, J. S. Wall, A. Böckmann, P. Güntert, B. H. Meier, and R. Riek, "Atomic-resolution structure of a disease-relevant Aβ(1–42) amyloid fibril," Proc. Natl. Acad. Sci. U. S. A. **113**, E4976–E4984 (2016).

[23]M. Schmidt, C. Sachse, W. Richter, C. Xu, M. Fandrich, and N. Grigorieff, "Comparison of Alzheimer Abeta(1-40) and Abeta(1-42) amyloid fibrils reveals similar protofilament structures," Proc. Natl. Acad. Sci. U. S. A. **106**, 19813–19818 (2009).

[24]M. H. M. Olsson, C. R. Søndergaard, M. Rostkowski, and J. H. Jensen, "PROPKA3: Consistent treatment of internal and surface residues in empirical pKa predictions," J. Chem. Theory Comput. **7**, 525–537 (2011).

[25]W. Humphrey, A. Dalke, and K. Schulten, "VMD: Visual molecular dynamics," J. Mol. Graphics Modell. **14**, 33–38 (1996).

[26]B. Hess, C. Kutzner, D. van der Spoel, and E. Lindahl, "GROMACS 4: Algorithms for highly efficient, load-balanced, and scalable molecular simulation," J. Chem. Theory Comput. **4**, 435–447 (2008).

[27]A. D. MacKerell, D. Bashford, M. Bellott, R. L. Dunbrack, J. D. Evanseck, M. J. Field, S. Fischer, J. Gao, H. Guo, S. Ha, D. Joseph-McCarthy, L. Kuchnir, K. Kuczera, F. T. K. Lau, C. Mattos, S. Michnick, T. Ngo, D. T. Nguyen, B. Prodhom, W. E. Reiher, B. Roux, M. Schlenkrich, J. C. Smith, R. Stote, J. Straub, M. Watanabe, J. Wiorkiewicz-Kuczera, D. Yin, and M. Karplus, "All-atom empirical potential for molecular modeling and dynamics studies of proteins," J. Phys. Chem. B **102**, 3586–3616 (1998).

[28]P. Bjelkmar, P. Larsson, M. A. Cuendet, B. Hess, and E. Lindahl, "Implementation of the CHARMM force field in GROMACS: Analysis of protein stability effects from correction maps, virtual interaction sites, and water models," J. Chem. Theory Comput. **6**, 459–466 (2010).

[29]W. L. Jorgensen, J. Chandrasekhar, J. D. Madura, R. W. Impey, and M. L. Klein, "Comparison of simple potential functions for simulating liquid water," J. Chem. Phys. **79**, 926–935 (1983).

[30]G. Bussi, D. Donadio, and M. Parrinello, "Canonical sampling through velocity rescaling," J. Chem. Phys. **126**, 014101 (2007).

[31]M. Parrinello and A. Rahman, "Polymorphic transitions in single crystals: A new molecular dynamics method," J. Appl. Phys. **52**, 7182–7190 (1981).

[32]T. Darden, D. York, and L. Pedersen, "Particle mesh Ewald—An N.log(N) method for Ewald sums in large systems," J. Chem. Phys. **98**, 10089–10092 (1993).

[33]W. Kabsch and C. Sander, "Dictionary of protein secondary structure: Pattern recognition of hydrogen-bonded and geometrical features," Biopolymers **22**, 2577–2637 (1983).

[34]G. M. Torrie and J. P. Valleau, "Nonphysical sampling distributions in Monte Carlo free-energy estimation: Umbrella sampling," J. Comput. Phys. **23**, 187–199 (1977).

[35]C. Dellago, P. G. Bolhuis, and D. Chandler, "Efficient transition path sampling: Application to Lennard-Jones cluster rearrangements," J. Chem. Phys. **108**, 9236–9245 (1998).

[36]S. Kumar, D. Bouzida, R. H. Swendsen, P. A. Kollman, and J. M. Rosenberg, "The weighted histogram analysis method for free-energy calculations on biomolecules. 1. The method," J. Comput. Chem. **13**, 1011–1021 (1992).

[37]J. S. Hub, B. L. de Groot, and D. van der Spoel, "g_wham—A free weighted histogram analysis implementation including robust error and autocorrelation estimates," J. Chem. Theory Comput. **6**, 3713–3720 (2010).

[38]B. Efron, "1977 Rietz lecture—Bootstrap methods: Another look at the Jackknife," Ann. Stat. **7**, 1–26 (1979).

[39]T. S. Lee, B. K. Radak, M. Huang, K. Y. Wong, and D. M. York, "Roadmaps through free energy landscapes calculated using the multidimensional vFEP approach," J. Chem. Theory Comput. **10**, 24–34 (2014).

[40]W. H. Xi, W. H. Wang, G. Abbott, and U. H. E. Hansmann, "Stability of a recently found triple-beta-stranded Aβ1-42 fibril motif," J. Phys. Chem. B **120**, 4548–4557 (2016).